IMPROVED ANALYTICAL MODEL FOR SURFACE-MOUNTED PM MOTORS CONSIDERING SLOTTING EFFECTS AND ARMATURE REACTION

Thierry Lubin, Smail Mezani, Abderrezak Rezzoug

Progress In Electromagnetics Research B, Vol. 25, 293–314, 2010

IMPROVED ANALYTICAL MODEL FOR SURFACE-MOUNTED PM MOTORS CONSIDERING SLOTTING EFFECTS AND ARMATURE REACTION

T. Lubin, S. Mezani, and A. Rezzoug

Groupe de Recherche en Electrotechnique et Electronique de Nancy (GREEN)
University Henri Poincaré
Nancy 54506, France

Abstract—This paper presents an exact analytical method for the computation of the magnetic field distribution in surface-mounted permanent-magnet (PM) motors for any pole and slot combinations including fractional slot machines. The proposed model takes into account the slotting effect and the armature reaction magnetic field. The analytical method is based on the resolution of the two-dimensional Laplace's and Poisson's equations in polar coordinates (by the separation of variables technique) for each subdomain, i.e., magnet, airgap and slots. Magnetic field distributions, back electromotive force and electromagnetic torque (cogging torque and load torque) computed with the proposed analytical method are verified with those obtained from finite element analyses.

1. INTRODUCTION

An accurate determination of the magnetic field distribution in the airgap of permanent magnets machines is necessary to evaluate the machine performances such as electromagnetic torque or back electromotive force (EMF). The presence of stator slots has a large influence on the airgap magnetic field distribution and therefore on the motor performances (noise and vibrations due to radial forces, magnet eddy-current losses ...).

The airgap magnetic field computation with slotting effects can be evaluated by numerical methods like finite elements or by analytical

Received 12 August 2010, Accepted 7 September 2010, Scheduled 15 September 2010
Corresponding author: T. Lubin (thierry.lubin@green.uhp-nancy.fr).

methods. Analytical methods are useful tools for a first evaluation of electrical motors performances and for design optimization. Two analytical methods are mainly developed in the literature, the first one uses conformal mapping [2–6] and the second one the subdomains method by Fourier analysis [7–19]. Recent comprehensive reviews of analytical methods can be founded in [11] and [18] and will not be developed once again here.

Although several papers have been published on the computation of the no-load airgap magnetic field in permanent magnet machines with slotting effect, very few papers have been devoted to armature reaction analysis [8, 16]. In [8], the armature reaction field is calculated from the product of the magnetic field due to the stator winding when slotting is neglected by a relative permeance function of the slotted airgap region. In this model, the winding current is replaced by a current sheet located at the armature bore radius. In [16], an improved model based on the exact analytical solution of armature reaction magnetic field is developed. However, the interaction between the magnetic field produced by permanent magnets and the armature reaction magnetic field is not studied, so the computation of the electromagnetic torque in the motor is not developed.

The authors propose here an exact analytical solution of the magnetic field distribution in the airgap of a surface mounted PM machine based on the subdomain method accounting for slotting effects and armature reaction. Laplace's and Poisson's equations are solved in each subdomain (airgap, magnet and slots) and the solution is obtained using boundary and interface conditions. The proposed model is very general and can be used for surface mounted PM machines with any pole and slot number combinations including fractional slot machines with distributed or concentrated windings.

The paper is organized as follows. The problem description and the assumptions of the model are presented in Section 2. Section 3 describes the analytical method for magnetic field calculation in the airgap, permanent magnets and in the slot subdomains. The back-EMF and torque expressions are developed in Section 4. The analytical results are then verified with the finite-element method in Section 5 for two PM machines including a fractional slot machine under no-load and load conditions.

2. PROBLEM DESCRIPTION AND ASSUMPTIONS

The geometric representation of the model is shown in Fig. 1. The geometrical parameters are the inner radius of the rotor yoke R_1, the radius of the PM surface R_2, the inner and outer radii of the slots R_3

and R_4 respectively. The pole-arc to pole-pitch ratio of the PM rotor is α and the number of pole pairs is p. The stator has Q slots with a homogeneous current density distribution J_i in each slot.

The slot opening angle is β. The angular position of the ith stator slot is defined as

$$\theta_i = -\frac{\beta}{2} + \frac{2i\pi}{Q} \quad \text{with} \quad 1 \leq i \leq Q \tag{1}$$

The following assumptions are considered:

- The machine is assumed infinitely long so the end effects are neglected.
- The current density has only one component along the z-axis.
- Stator and rotor iron cores are infinitely permeable.
- Radially magnetized magnets with a relative recoil permeability $\mu_r = 1$.
- The stator slots have radial sides.

As shown in Fig. 1, the whole domain is divided into three subdomains: the rotor PMs subdomain (regions I), the airgap subdomain (regions II) and the Q stator slots subdomains (regions i). The ith slot subdomain shape is shown in Fig. 2. The subdomains I and II have annular shapes.

Due to the presence of electrical current in the slots, a magnetic vector potential formulation is used in 2D polar coordinates to describe the problem. According to the adopted assumptions, the magnetic vector potential has only one component along the z-direction and only depends on the r and θ coordinates. The magnetic vector potential in the different subdomains is noted

$A_I = A_I(r,\theta)e_z$ for the rotor PMs subdomain
$A_{II} = A_{II}(r,\theta)e_z$ for the airgap subdomain
$A_i = A_i(r,\theta)e_z$ for the ith slot subdomain.

3. ANALYTICAL MODEL

By using the separation of variables technique, we now consider the solution of Poisson's equations for the slots (with current density) and PMs subdomains and Laplace's equation in the airgap subdomain. For the sake of clarity of the general solutions in the different subdomains, we introduce the following functions of three dummy variables u, v and w

$$P_w(u,v) = \left(\frac{u}{v}\right)^w + \left(\frac{v}{u}\right)^w \tag{2}$$

$$E_w(u,v) = \left(\frac{u}{v}\right)^w - \left(\frac{v}{u}\right)^w \tag{3}$$

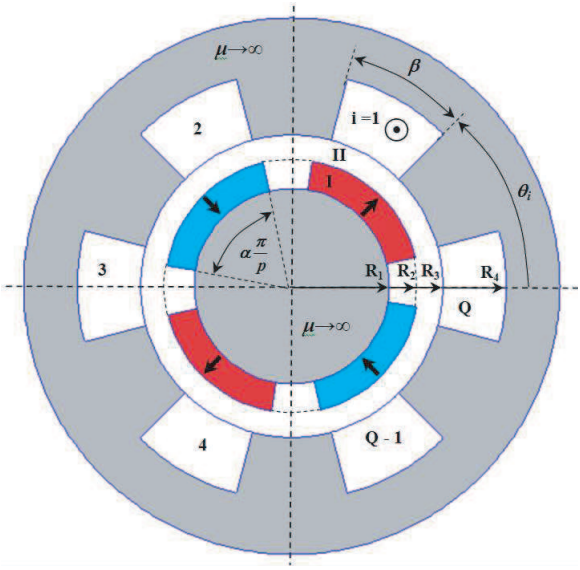

Figure 1. Geometry of the studied surface-mounted PM motor with the different subdomains ($Q = 6$ and $p = 2$).

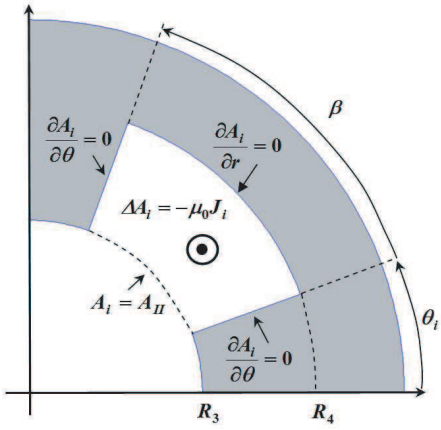

Figure 2. ith slot subdomain with its boundary conditions.

3.1. Solution of Poisson's Equation in the ith Slot Subdomain (Region i)

The ith slot domain and the associated boundary conditions are shown in Fig. 2. We have to solve Poisson's equation in a domain of inner

radius R_3 and outer radius R_4 delimited by the angles θ_i and $\theta_i + \beta$

$$\frac{\partial^2 A_i}{\partial r^2} + \frac{1}{r}\frac{\partial A_i}{\partial r} + \frac{1}{r^2}\frac{\partial^2 A_i}{\partial \theta^2} = -\mu_0 J_i \quad \text{for} \quad \begin{cases} R_3 \le r \le R_4 \\ \theta_i \le \theta \le \theta_i + \beta \end{cases} \tag{4}$$

where J_i is the current density in slot i.

The tangential component of the magnetic field at the sides and at the bottom of the slot being null (iron with infinite permeability), the boundary conditions for the ith slot are

$$\left.\frac{\partial A_i}{\partial \theta}\right|_{\theta=\theta_i} = 0 \quad \text{and} \quad \left.\frac{\partial A_i}{\partial \theta}\right|_{\theta=\theta_i+\beta} = 0 \tag{5}$$

$$\left.\frac{\partial A_i}{\partial r}\right|_{r=R_4} = 0 \tag{6}$$

The continuity condition between the ith slot and the airgap leads to

$$A_i(R_3, \theta) = A_{II}(R_3, \theta) \tag{7}$$

The general solution of (4) can be found by using the method of the separation of variables. According to the superposition principle, the general solution of (4) is the sum of the general solution of the corresponding Laplace's equation and a particular solution [1]. Taking into account the boundary conditions (5) and (6), the solution can be written as [17]

$$\begin{aligned} A_i(r,\theta) \;=\; & A_0^i + \frac{1}{4}\mu_0 J_i \left(R_3^2 - r^2\right) + \frac{1}{2}R_4^2 \mu_0 J_i \ln\left(\frac{r}{R_3}\right) \\ & + \sum_{k=1}^{\infty} A_k^i \frac{P_{k\pi/\beta}(r, R_4)}{P_{k\pi/\beta}(R_3, R_4)} \cos\left(\frac{k\pi}{\beta}(\theta - \theta_i)\right) \end{aligned} \tag{8}$$

where the function $P_{k\pi/\beta}(r, R_4)$ is defined by (2).

The constants A_0^i and A_k^i are determined by using a Fourier series expansion of the airgap magnetic vector potential A_{II} given by (15) over the slot interval $[\theta_i,\, \theta_i + \beta]$ at $r = R_3$.

$$A_0^i = \frac{1}{\beta} \int_{\theta_i}^{\theta_i+\beta} A_{II}(R_3, \theta) d\theta \tag{9}$$

$$A_k^i = \frac{2}{\beta} \int_{\theta_i}^{\theta_i+\beta} A_{II}(R_3, \theta) \cos\left(\frac{k\pi}{\beta}(\theta - \theta_i)\right) d\theta \tag{10}$$

The expressions of the coefficients A_0^i and A_k^i are given in the appendix.

3.2. Solution of Laplace's Equation in the AirGap Subdomain (Region II)

The airgap subdomain and the associated boundary conditions are shown in Fig. 3. The problem to solve is

$$\frac{\partial^2 A_{II}}{\partial r^2} + \frac{1}{r}\frac{\partial A_{II}}{\partial r} + \frac{1}{r^2}\frac{\partial^2 A_{II}}{\partial \theta^2} = 0 \quad \text{for} \quad \begin{cases} R_2 \leq r \leq R_3 \\ 0 \leq \theta \leq 2\pi \end{cases} \tag{11}$$

The continuity of the tangential component of the magnetic field at $r = R_2$ leads to

$$\left.\frac{\partial A_{II}}{\partial r}\right|_{r=R_2} = \left.\frac{\partial A_I}{\partial r}\right|_{r=R_2} \tag{12}$$

The boundary condition at $r = R_3$ is more difficult to handle because of the existence of the slots as shown in Fig. 1. Considering the continuity of the tangential magnetic field at the interface between the slots and the airgap and considering that the tangential magnetic field is equal to zero elsewhere (infinite permeability of the ferromagnetic pieces), the boundary condition at $r = R_3$ can be written as

$$\left.\frac{\partial A_{II}}{\partial r}\right|_{r=R_3} = f(\theta) \tag{13}$$

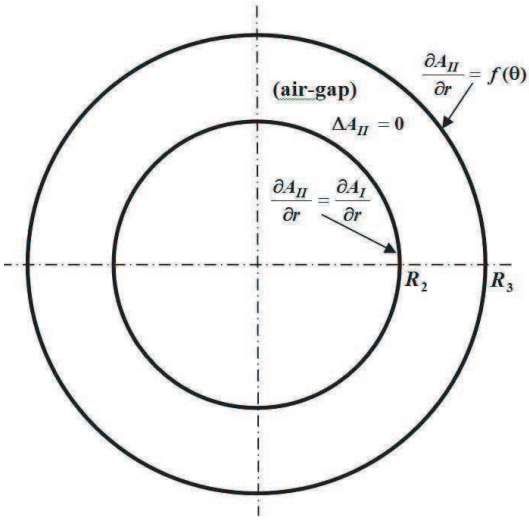

Figure 3. Airgap subdomain (region II) with its boundary conditions.

with

$$f(\theta) = \begin{cases} \left.\frac{\partial A_i}{\partial r}\right|_{r=R_3} & \forall\theta \in [\theta_{\rm i}, \theta_i + \beta] \\ 0 & \text{elsewhere} \end{cases} \tag{14}$$

where $A_i(r,\theta)$ is the magnetic vector potential in the ith slot given by (8).

With the boundary conditions (12) and (13), the general solution of the magnetic vector potential in the airgap can be written as

$$A_{II}(r,\theta) = \sum_{n=1}^{\infty}\left(A_n^{II}\frac{R_2}{n}\frac{P_n(r,R_3)}{E_n(R_2,R_3)} + B_n^{II}\frac{R_3}{n}\frac{P_n(r,R_2)}{E_n(R_3,R_2)}\right)\cos(n\theta) + \sum_{n=1}^{\infty}\left(C_n^{II}\frac{R_2}{n}\frac{P_n(r,R_3)}{E_n(R_2,R_3)} + D_n^{II}\frac{R_3}{n}\frac{\mathrm{P}_n(r,R_2)}{E_n(R_3,R_2)}\right)\sin(n\theta) \tag{15}$$

where n is a positive integer, $P_n(r,R_3)$ and $E_n(R_2,R_3)$ are defined by (2) and (3). The coefficients A_n^{II}, B_n^{II}, C_n^{II} and D_n^{II} are determined using Fourier series expansion of $\left.\frac{\partial A_I}{\partial r}\right|_{R_2}$ and $f(\theta)$ over the airgap interval [0, 2π]

$$A_n^{II} = \frac{2}{2\pi}\int_0^{2\pi}\left.\frac{\partial A_I}{\partial r}\right|_{R_2}\cos(n\theta)d\theta \tag{16}$$

$$B_n^{II} = \frac{2}{2\pi}\int_0^{2\pi} f(\theta)\cos(n\theta)d\theta \tag{17}$$

$$C_n^{II} = \frac{2}{2\pi}\int_0^{2\pi}\left.\frac{\partial A_I}{\partial r}\right|_{R_2}\sin(n\theta)d\theta \tag{18}$$

$$D_n^{II} = \frac{2}{2\pi}\int_0^{2\pi} f(\theta)\sin(n\theta)d\theta \tag{19}$$

The expressions of the coefficients A_n^{II}, B_n^{II}, C_n^{II} and D_n^{II} are given in the appendix.

The radial and tangential flux densities in the airgap are deduced from the magnetic vector potential by

$$B_{IIr} = \frac{1}{r}\frac{\partial A_{II}}{\partial\theta} \quad B_{II\theta} = -\frac{\partial A_{II}}{\partial r} \tag{20}$$

The radial and the tangential components of the magnetic flux in the inner air-gap are then

$$B_{IIr}(r,\theta)=+\sum_{n=1}^{\infty}-\left(A_n^{II}\frac{R_2}{r}\frac{P_n(r,R_3)}{E_n(R_2,R_3)}+B_n^{II}\frac{R_3}{r}\frac{P_n(r,R_2)}{E_n(R_3,R_2)}\right)\sin(n\theta)$$
$$+\sum_{n=1}^{\infty}\left(C_n^{II}\frac{R_2}{r}\frac{P_n(r,R_3)}{E_n(R_2,R_3)}+D_n^{II}\frac{R_3}{r}\frac{P_n(r,R_2)}{E_n(R_3,R_2)}\right)\cos(n\theta) \quad (21)$$

$$B_{II\theta}(r,\theta)=+\sum_{n=1}^{\infty}-\left(A_n^{II}\frac{R_2}{r}\frac{E_n(r,R_3)}{E_n(R_2,R_3)}+B_n^{II}\frac{R_3}{r}\frac{E_n(r,R_2)}{E_n(R_3,R_2)}\right)\cos(n\theta)$$
$$+\sum_{n=1}^{\infty}-\left(C_n^{II}\frac{R_2}{r}\frac{E_n(r,R_3)}{E_n(R_2,R_3)}+D_n^{II}\frac{R_3}{r}\frac{E_n(r,R_2)}{E_n(R_3,R_2)}\right)\sin(n\theta) \quad (22)$$

3.3. Solution of Poisson's Equation in the PMs Subdomain (Region I)

The rotor PMs subdomain and the associated boundary conditions are shown in Fig. 4. The problem to solve (derived from Maxwell's equations) is

$$\frac{\partial^2 A_I}{\partial r^2}+\frac{1}{r}\frac{\partial A_I}{\partial r}+\frac{1}{r^2}\frac{\partial^2 A_I}{\partial \theta^2}=\frac{\mu_0}{r}\frac{\partial M_r}{\partial \theta} \quad \text{for} \quad \begin{cases} R_1 \le r \le R_2 \\ 0 \le \theta \le 2\pi \end{cases} \quad (23)$$

where μ_0 is the permeability of the vacuum and M_r is the radial magnetization of the magnets. The boundary conditions at $r = R_1$ and $r = R_2$ are respectively

$$\left.\frac{\partial A_I}{\partial r}\right|_{r=R_1}=0 \quad (24)$$

$$A_I(R_2,\theta)=A_{II}(R_2,\theta) \quad (25)$$

The radial magnetization distribution M_r is plotted in Fig. 5, where B_r is the remanence of the magnets and δ is the position of the rotor. The radial magnetization can be expressed in Fourier's series and replaced in (23).

Taking into account the boundary conditions (24) and (25), the general solution of the magnetic vector potential in the PMs subdomain can be written as

$$A_I(r,\theta) = \sum_{n=1}^{\infty}\left(A_n^I\frac{\mathrm{P}_n(r,R_1)}{\mathrm{P}_n(R_2,R_1)}+X_n(r)\cos(n\delta)\right)\cos(n\theta)$$
$$+\sum_{n=1}^{\infty}\left(C_n^I\frac{\mathrm{P}_n(r,R_1)}{\mathrm{P}_n(R_2,R_1)}+X_n(r)\sin(n\delta)\right)\sin(n\theta) \quad (26)$$

where

$$X_n(r) = -\frac{\mathrm{P}_n(r, R_1)}{\mathrm{P}_n(R_2, R_1)}\left(\frac{R_1}{n}\left(\frac{R_1}{R_2}\right)^n f_n'(R_1) + f_n(R_2)\right) + \left(\frac{R_1}{n}\left(\frac{R_1}{r}\right)^n f_n'(R_1) + f_n(r)\right) \quad (27)$$

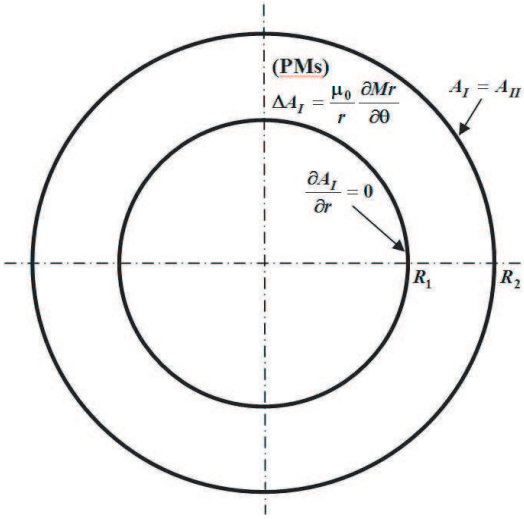

Figure 4. PMs subdomain (region I) with its boundary conditions.

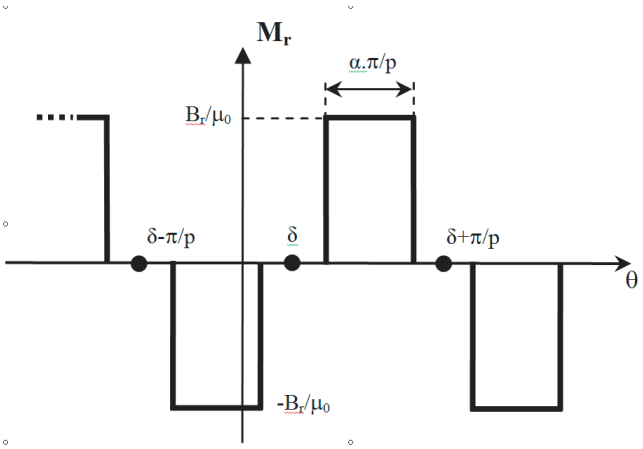

Figure 5. Magnetization distribution along θ-direction (PMs rotor).

and

$$f_n(r)=\begin{cases}\frac{4B_r p}{\pi(1-n^2)} r\cos\left(\frac{n\pi}{2p}(1-\alpha)\right) & if\ n=jp\ \ with\ \ j=1,3\ldots \\ \frac{2B_r}{\pi} r\ln(r)\cos\left(\frac{\pi}{2}(1-\alpha)\right) & if\ n=p=1 \\ 0 & otherwise\end{cases} \tag{28}$$

where n is a positive integer and p is the number of pole-pairs of the PMs rotor

It is important to note here that the magnetic vector potential solution (26) contains some harmonic terms which are not multiple of the pole pairs number p. This is due to the presence of the slots.

The coefficients A_n^I and C_n^I are determined using a Fourier series expansion of $A_{II}(R_2,\theta)$ over the interval [0, 2π]

$$A_n^I = \frac{2}{2\pi}\int_0^{2\pi} A_{II}(R_2,\theta)\cos(n\theta)d\theta \tag{29}$$

$$C_n^I = \frac{2}{2\pi}\int_0^{2\pi} A_{II}(R_2,\theta)\sin(n\theta)d\theta \tag{30}$$

The expressions of the coefficients A_n^I and C_n^I are given in the appendix.

4. BACK-EMF AND TORQUE CALCULATION

4.1. Electromagnetic Torque Expression

The electromagnetic torque is obtained using the Maxwell stress tensor. A circle of radius R_e in the airgap subdomain is taken as the integration path so the electromagnetic torque is expressed as follows

$$T_e = \frac{LR_e^2}{\mu_0}\int_0^{2\pi} B_{IIr}(R_e,\theta)B_{II\theta}(R_e,\theta)d\theta \tag{31}$$

where L is the axial length of the motor. According to (21) and (22), the analytical expression for the electromagnetic torque becomes

$$T_e = \frac{\pi LR_e^2}{\mu_0}\sum_{n=1}^{\infty}(W_nX_n + Y_nZ_n) \tag{32}$$

where

$$\begin{aligned} W_n &= -A_n^{II}\frac{R_2}{R_e}\frac{P_n(R_e,R_3)}{E_n(R_2,R_3)} - B_n^{II}\frac{R_3}{R_e}\frac{P_n(R_e,R_2)}{E_n(R_3,R_2)} \\ X_n &= -C_n^{II}\frac{R_2}{R_e}\frac{E_n(R_e,R_3)}{E_n(R_2,R_3)} - D_n^{II}\frac{R_3}{R_e}\frac{E_n(R_e,R_2)}{E_n(R_3,R_2)} \\ Y_n &= C_n^{II}\frac{R_2}{R_e}\frac{P_n(R_e,R_3)}{E_n(R_2,R_3)} + D_n^{II}\frac{R_3}{R_e}\frac{P_n(R_e,R_2)}{E_n(R_3,R_2)} \\ Z_n &= -A_n^{II}\frac{R_2}{R_e}\frac{E_n(R_e,R_3)}{E_n(R_2,R_3)} - B_n^{II}\frac{R_3}{R_e}\frac{E_n(R_e,R_2)}{E_n(R_3,R_2)} \end{aligned} \tag{33}$$

4.2. Back-EMF Expression

In order to compute the back-EMF of a 3-phase motor, we first determine at a given rotor position δ, the flux over each slot i of cross section S_{slot}. We have supposed that the current density is uniformly distributed over the slot area, so the vector potential can be averaged over the slot area to represent the coil

$$\varphi_i = \frac{L}{S_{slot}}\iint_{S_{slot}} A_i(r,\theta)rdrd\theta \text{ with } S_{slot} = \beta\frac{\left(R_4^2 - R_3^2\right)}{2} \tag{34}$$

where L is the machine axial length. The vector potential $A_i(r,\theta)$ is given by (8). The development of (34) gives

$$\varphi_i = LA_0^i + J_i\frac{\beta\mu_0 L}{2S_{slot}}\left(-\frac{3}{8}R_4^4 + \frac{1}{2}R_4^4\ln\left(\frac{R_4}{R_3}\right) + \frac{1}{2}R_4^2R_3^2 - \frac{1}{8}R_3^4\right) \tag{35}$$

Under no-load condition ($J_i = 0$), the flux over each slot becomes

$$\varphi_i = LA_0^i \tag{36}$$

The phase flux vector is given by

$$\begin{pmatrix} \Psi_a \\ \Psi_b \\ \Psi_c \end{pmatrix} = n_{turn}[C]\begin{pmatrix} \varphi_1 & \varphi_2 & \cdot & \varphi_i & \cdot & \varphi_{Q-1} & \varphi_Q \end{pmatrix}^t \tag{37}$$

where n_{turn} is the number of turns in series per phase and $[C]$ is a connection matrix (of dimension $3 \times Q$) that represents the stator windings distribution in the slots. For example, Fig. 6 shows a three phases windings distribution for a stator with 12 slots, a number of pole-pairs $p = 1$ and a double-layer winding with a coil pitch equals to 5 slots.

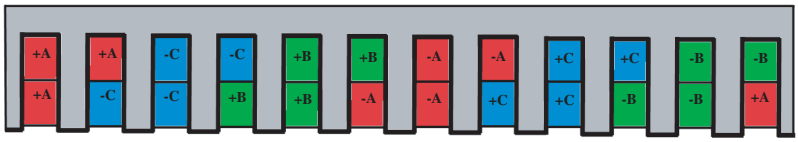

Figure 6. Double-layer windings distribution for a three phases machine with 12 slots and $p = 1$.

The corresponding connection matrix (of the slots with respect to the phases) is

$$[C] = \begin{bmatrix} 2 & 1 & 0 & 0 & 0 & -1 & -2 & -1 & 0 & 0 & 0 & 1 \\ 0 & 0 & 0 & 1 & 2 & 1 & 0 & 0 & 0 & -1 & -2 & -1 \\ 0 & -1 & -2 & -1 & 0 & 0 & 0 & 1 & 2 & 1 & 0 & 0 \end{bmatrix} \quad (38)$$

The three-phase back-EMF vector is computed by

$$\begin{pmatrix} E_a \\ E_b \\ E_c \end{pmatrix} = \Omega \frac{d}{d\delta} \begin{pmatrix} \Psi_a \\ \Psi_b \\ \Psi_c \end{pmatrix} \quad (39)$$

where Ω is the rotating speed of the rotor.

Using (A11), (A12) and (A19) (see the appendix), an analytical expression can be derived for the back-EMF as follow

$$\begin{pmatrix} E_a \\ E_b \\ E_c \end{pmatrix} = \Omega L n_{turn} [C] \frac{d}{d\delta} \left(A_0^i\right)^t \quad (40)$$

5. VERIFICATION OF THE ANALYTICAL RESULTS USING FEM

5.1. Application Example 1: Integer Slot/pole Machine

The analytical method described above is applied to compute a three-phase PM motor having an integer slot per pole and per phase ratio i.e., 4 poles and 24 slots ($q = 2$). A double-layer winding with a coil pitch equals to 5 slots is used. The connection matrix for 1 pole-pair is the one given by (38). The geometrical parameters of the motor are given in Table 1. The analytical solutions in the airgap, in the PMs and in the slots domains have been computed with a finite number of harmonic terms N and K as indicated in Table 1.

In order to validate the proposed analytical model, the analytical results have been compared with 2D finite element simulations obtained using FEMM software [20]. The finite-element solutions were

Table 1. Parameters of the studied PMs Motor.

Symbol	Quantity	Value
R_1	Inner radius of the rotor yoke	3 cm
R_2	Radius of the PMs rotor surface	4 cm
R_3	Stator bore radius	4.2 cm
R_4	Outer radius of the slot	5.7 cm
L	Axial length	10 cm
β	Slot opening	7.5°
α	PMs pole-arc to pole-pitch ratio	0.85
B_r	Remanence of the permanent magnets	1.2 T
p	Pole-pairs PMs rotor	2
Q	Number of stator slots	24
J_{rms}	RMS current density	5 A/mm^2
N	Number of harmonics used for magnetic field calculation in the airgap and PMs domains	50
K	Number of harmonics used for magnetic field calculation in the slot domain	50

obtained by imposing the natural Neumann boundary condition at the surface of the stator and rotor iron cores. The mesh in the different subdomains has been refined until convergent results are obtained.

5.1.1. Results under No-load Conditions ($J_{rms} = 0$)

Figure 7 presents the radial and tangential flux density distribution along a circle in the middle of the airgap. A good accordance is seen between the finite element method (FEM) and the analytical computations. The effects of the stator slotting can be clearly observed from this figure.

The back-EMF waveform for $n_{turn} = 1$ is presented in Fig. 8. The computation is done for a rotating speed $\Omega = 1500$ rpm. The maximum value of the back-EMF is around 9 V. The analytical and numerical predictions are close to less than 1%. An important characteristic of a PM motor is the cogging torque. For a slot opening corresponding to half a tooth pitch, viz. $\beta = 7.5°$, the obtained cogging torque is shown in Fig. 9. The cogging torque waveform obtained from FEM is very similar to the one issued from the analytical calculation.

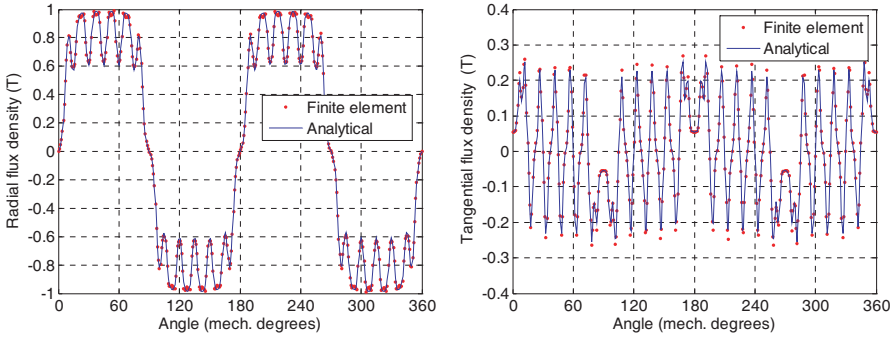

Figure 7. Radial (a) and tangential (b) flux density distribution at no load in the middle of the airgap ($Q = 24$ slots).

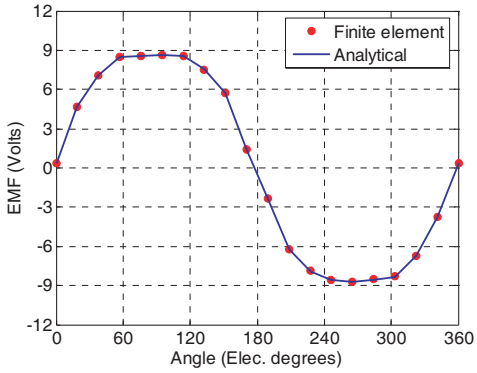

Figure 8. Per turn phase back-EMF ($Q = 24$ slots).

To show the influence of the slot opening on the cogging torque, we have plotted in Fig. 10 the cogging torque waveforms for several values of the slot opening β. As expected, the cogging torque decreases for lower values of β.

5.1.2. Results under Load Conditions ($J_{rms} = 5\,\mathrm{A/mm^2}$)

For a RMS current density $J_{rms} = 5\,\mathrm{A/mm^2}$ in the slots, Fig. 11 presents the radial and tangential flux density distribution along a circle in the middle of the airgap. Compared to the no-load results of Fig. 7, one can see the influence of the armature reaction on both the radial and the tangential flux densities.

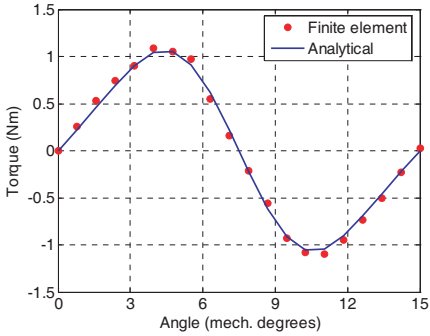

Figure 9. Cogging torque for $\beta = 7.5°$ ($Q = 24$ slots).

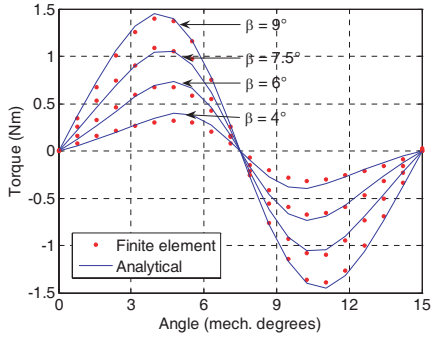

Figure 10. Cogging torque for several slot opening values ($Q = 24$ slots).

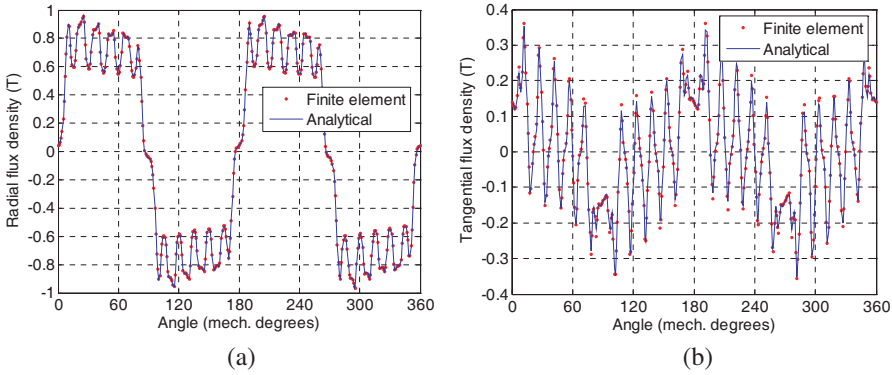

Figure 11. Radial (a) and tangential (b) flux density distribution in the middle of the airgap under load conditions ($J_{rms} = 5\,\mathrm{A/mm^2}$) and ($Q = 24$ slots).

The static torque is presented in Fig. 12. Compared to the FE simulations, one can see that the analytical model well tracks the torque ripples which are mainly due to the cogging torque. It can be seen that the cogging torque (Fig. 9) represents almost 3% of the stall torque of the motor. It is worthy to notice that these ripples will be less important if a slot isthmus is present as usually done in low to medium power machines.

5.2. Application Example 2: Fractional Slot/pole Machine

Another example is considered in this section for a fractional slot machine ($q = 1.25$). The same geometrical parameters as in Table 1

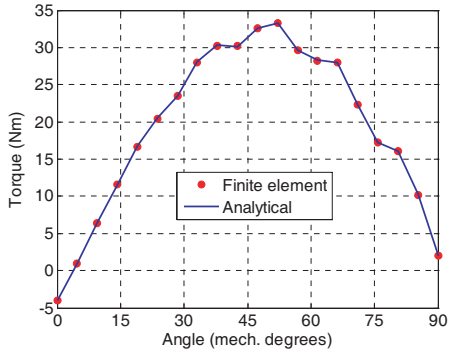

Figure 12. Static torque versus rotor position ($J_{rms} = 5\,\mathrm{A/mm^2}$) and (Q=24 slots).

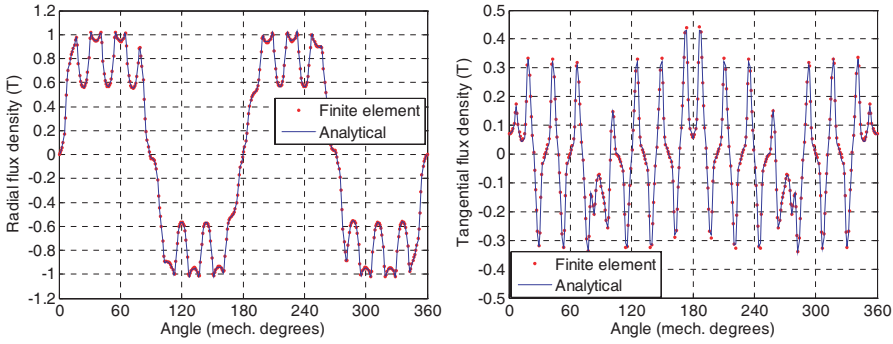

(a) (b)

Figure 13. Radial (a) and tangential (b) flux density distribution at no load in the middle of the airgap ($Q = 15$ slots).

are used except for the number of slots and the slot opening which are now $Q = 15$ and $\beta = 12°$. This fractional slot machine has a double-layer winding with a coil pitch equals to 3 slots. The corresponding connection matrix is

$$[C] = \begin{bmatrix} 2 & 1 & 0 & -1 & -2 & 0 & 0 & 1 & 1 & 0 & 0 & -1 & -1 & 0 & 0 \\ 0 & -1 & -1 & 0 & 0 & 2 & 1 & 0 & -1 & -2 & 0 & 0 & 1 & 1 & 0 \\ 0 & 0 & 1 & 1 & 0 & 0 & -1 & -1 & 0 & 0 & 2 & 1 & 0 & -1 & -2 \end{bmatrix} \quad (41)$$

5.2.1. Results under No-load Conditions ($J_{rms} = 0$)

Figure 13 shows the flux density distribution (radial and tangential components) along a circle in the middle of the airgap. As expected,

the flux density waveforms are not p-periodic for this fractional slot machine.

The back-emf waveform (with $n_{turn} = 1$) is presented in Fig. 14. The computation is done for a rotating speed $\Omega = 1500\,\text{rpm}$. Compared to the machine with $Q = 24$, the maximum value of the emf is around 5 V in this case instead of 9 V in Fig. 8. This difference is due to the coil pitch which is equal to 3 slots for the 15-slot machine and 5 slots for the 24-slot machine.

The cogging torque is given in Fig. 15. As it can be seen, its maximum value is much lower than the one given for the 24-slot machine (Fig. 9). Indeed, this is typical for fractional slot machines for which the cogging torque has a high harmonic order (its period is $360°/LCM(Q, 2p) = 6°$, where LCM is the lowest common multiple).

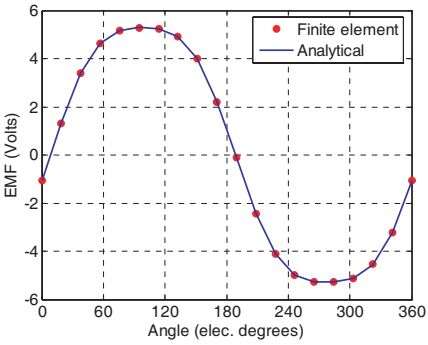

Figure 14. Per turn phase back-EMF.

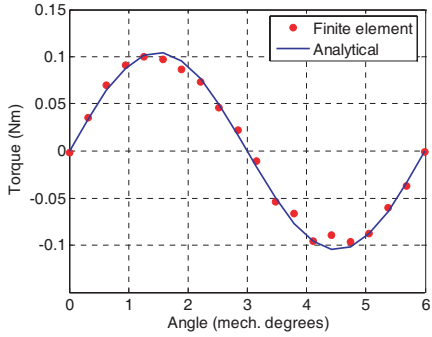

Figure 15. Cogging torque for $\beta = 12°$.

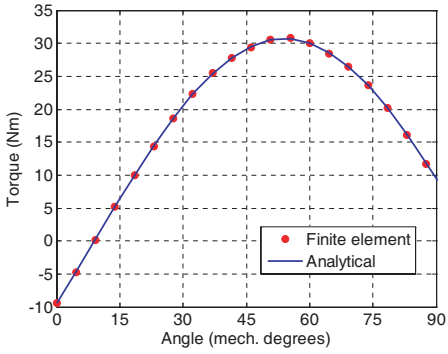

Figure 16. Static torque versus rotor position ($J_{rms} = 5\,\text{A/mm}^2$) and ($Q = 15$ slots).

5.2.2. Results under Load Conditions ($J_{rms} = 5\,\mathrm{A/mm^2}$)

For a RMS current density $J_{rms} = 5\,\mathrm{A/mm^2}$, the static torque is presented in Fig. 16. It can be seen that the torque is ripple free. The maximum torque is comparable to the one obtained for the 24-slot machine (Fig. 12). Once again, the analytical and FE results are in close agreement.

6. CONCLUSION

In this paper, a new analytical method for computing the airgap field distribution in PMs motors considering slotting effects and armature reaction field has been presented. Laplace's and Poisson's equations in polar coordinates have been solved by the technique of separation of variables in the different subdomains. The proposed model can be used for any pole and slot combinations including fractional slot winding machines as shown in the paper. Flux density distribution, back-EMF and torque computations for no-load and load conditions are in close agreement with those issued from finite element predictions. Compared to numerical approaches like FEM, the proposed analytical model is less computational time consuming. Hence, it may be used as a tool for the first stage of the design and optimization of PM motors. With this approach, sensitivity analyses and the impact of the different parameters on the machine design can be evaluated rapidly (under magnetically linear conditions).

APPENDIX A.

For the determination of the integration coefficients, we have to calculate integrals of the form

$$f(k,n,i) = \int_{\theta_i}^{\theta_i+\beta} \cos(n\theta)\cos\left(\frac{k\pi}{\beta}(\theta-\theta_i)\right)d\theta \qquad \text{(A1)}$$

$$g(k,n,i) = \int_{\theta_i}^{\theta_i+\beta} \sin(n\theta)\cos\left(\frac{k\pi}{\beta}(\theta-\theta_i)\right)d\theta \qquad \text{(A2)}$$

$$r(n,i) = \int_{\theta_i}^{\theta_i+\beta} \cos(n\theta)d\theta \tag{A3}$$

$$s(n,i) = \int_{\theta_i}^{\theta_i+\beta} \sin(n\theta)d\theta \tag{A4}$$

The development of (A1) and (A2) gives the following functions that will be used in the expressions of the Fourier coefficients

— for $k\pi \neq n\beta$

$$f(k,n,i) = \frac{-n\beta^2\left((-1)^k \sin n(\beta+\theta_i) - \sin(n\theta_i)\right)}{k^2\pi^2 - n^2\beta^2} \tag{A5}$$

$$g(k,n,i) = \frac{n\beta^2\left((-1)^k \cos n(\beta+\theta_i) - \cos(n\theta_i)\right)}{k^2\pi^2 - n^2\beta^2} \tag{A6}$$

— for $k\pi = n\beta$

$$f(k,n,i) = \frac{\beta}{2}\left(\cos(n\theta_i) + \frac{1}{2k\pi}\left(\sin n(\theta_i+2\beta) - \sin(n\theta_i)\right)\right) \tag{A7}$$

$$g(k,n,i) = \frac{\beta}{2}\left(\sin(n\theta_i) - \frac{1}{2k\pi}\left(\cos n(\theta_i+2\beta) - \cos(n\theta_i)\right)\right) \tag{A8}$$

The development of (A3) and (A4) gives the following functions

$$r(n,i) = \frac{1}{n}\left(\sin(n\theta_i + n\beta) - \sin(n\theta_i)\right) \tag{A9}$$

$$s(n,i) = \frac{1}{n}\left(-\cos(n\theta_i + n\beta) + \cos(n\theta_i)\right) \tag{A10}$$

• Expressions of the coefficients A_n^{II}, B_n^{II}, C_n^{II} and D_n^{II} for the airgap subdomain. The development of (16) and (18) gives

$$A_n^{II} = A_n^I \frac{n}{R_2}\frac{E_n(R_2,R_1)}{P_n(R_2,R_1)} + X_n'(R_2)\cos(n\delta) \tag{A11}$$

$$C_n^{II} = C_n^I \frac{n}{R_2}\frac{E_n(R_2,R_1)}{P_n(R_2,R_1)} + X_n'(R_2)\sin(n\delta) \tag{A12}$$

where δ is the position of the PM rotor and $X_n'(R_2) = \left.\frac{dX_n(r)}{dr}\right|_{r=R_2}$. $X_n(r)$ is given by (27).

The coefficient B_n^{II} and C_n^{II} defined in (17) and (19) can be written as

$$B_n^{II} = \frac{2}{2\pi}\sum_{i=1}^{Q}\int_{\theta_i}^{\theta_i+\beta} \left.\frac{\partial A_i}{\partial r}\right|_{r=R_3} \cos(n\theta)d\theta \tag{A13}$$

$$D_n^{II} = \frac{2}{2\pi} \sum_{i=1}^{Q} \int_{\theta_i}^{\theta_i+\beta} \left. \frac{\partial A_i}{\partial r} \right|_{r=R_3} \sin(n\theta) d\theta \tag{A14}$$

where Q is the number of stator slots. The development of (A13) and (A14) gives

$$\begin{aligned} B_n^{II} &= \sum_{i=1}^{Q} \frac{\mu_0 J_i}{2\pi} \left(\frac{R_4^2}{R_3} - R_3 \right) r(n,i) \\ &\quad + \sum_{i=1}^{Q} \sum_{k=1}^{\infty} A_k^i \frac{k}{\beta R_3} \frac{E_{k\pi/\beta}(R_3,R_4)}{P_{k\pi/\beta}(R_3,R_4)} f(k,n,i) \end{aligned} \tag{A15}$$

$$\begin{aligned} D_n^{II} &= \sum_{i=1}^{Q} \frac{\mu_0 J_i}{2\pi} \left(\frac{R_4^2}{R_3} - R_3 \right) s(n,i) \\ &\quad + \sum_{i=1}^{Q} \sum_{k=1}^{\infty} A_k^i \frac{k}{\beta R_3} \frac{E_{k\pi/\beta}(R_3,R_4)}{P_{k\pi/\beta}(R_3,R_4)} g(k,n,i) \end{aligned} \tag{A16}$$

• Expressions of the coefficients A_n^I and C_n^I, for the PMs subdomain (29) and (30)

$$A_n^I = A_n^{II} \frac{R_2}{n} \frac{\mathrm{P}_n(R_2,R_3)}{\mathrm{E}_n(R_2,R_3)} + B_n^{II} \frac{R_3}{n} \frac{2}{\mathrm{E}_n(R_3,R_2)} \tag{A17}$$

$$C_n^I = C_n^{II} \frac{R_2}{n} \frac{\mathrm{P}_n(R_2,R_3)}{\mathrm{E}_n(R_2,R_3)} + D_n^{II} \frac{R_3}{n} \frac{2}{\mathrm{E}_n(R_3,R_2)} \tag{A18}$$

• Expression of the coefficients A_0^i and A_k^i for the ith slot subdomain.

The treatment of (9) and (10) yields to the following linear relations

$$\begin{aligned} A_0^i = &\sum_{n=1}^{\infty} \left(A_n^{II} \frac{R_2}{n\beta} \frac{2}{E_n(R_2,R_3)} + B_n^{II} \frac{R_3}{n\beta} \frac{P_n(R_3,R_2)}{E_n(R_3,R_2)} \right) r(n,i) \\ &+ \sum_{n=1}^{\infty} \left(C_n^{II} \frac{R_2}{n\beta} \frac{2}{E_n(R_2,R_3)} + D_n^{II} \frac{R_3}{n\beta} \frac{P_n(R_3,R_2)}{E_n(R_3,R_2)} \right) s(n,i) \end{aligned} \tag{A19}$$

$$\begin{aligned} A_k^i = &\sum_{n=1}^{\infty} \left(A_n^{II} \frac{2R_2}{n\beta} \frac{2}{E_n(R_2,R_3)} + B_n^{II} \frac{2R_3}{n\beta} \frac{P_n(R_3,R_2)}{E_n(R_3,R_2)} \right) f(k,n,i) \\ &+ \sum_{n=1}^{\infty} \left(C_n^{II} \frac{2R_2}{n\beta} \frac{2}{E_n(R_2,R_3)} + D_n^{II} \frac{2R_3}{n\beta} \frac{P_n(R_3,R_2)}{E_n(R_3,R_2)} \right) g(k,n,i) \end{aligned} \tag{A20}$$

We have to solve a system of linear Equations (A11) to (A20) with the same number of unknowns. By rewriting the above equations in matrix and vectors form, a numerical solution can be found by using mathematical software (Matlab).

REFERENCES

1. Farlow, S. J., *Partial Differential Equations for Scientists and Engineers*, 414, Dover Publications, New York, 1993.
2. Sargos, F. M. and A. Rezzoug, "Analytical calculation of airgap magnetic field produced by inset permanent magnet rotor machine," *J. Physics III*, Vol. 1, 103–110, 1990 (in French).
3. Zhu, Z. Q. and D. Howe, "Instantaneous magnetic-field distribution in brushless permanent-magnet dc motor, part III: Effect of slotting," *IEEE Trans. Magn.*, Vol. 29, No. 1, 143–151, 1993.
4. Zarko, D., D. Ban, and T. A. Lipo, "Analytical calculation of magnetic field distribution in the slotted air gap of a surface permanent-magnet motor using complex relative air-gap permeance," *IEEE Trans. Magn.*, Vol. 42, No. 7, 1828–1837, 2006.
5. Markovic, M., M. Jufer, and Y. Perriard, "Reducing the cogging torque in brushless dc motors by using conformal mappings," *IEEE Trans. Magn.*, Vol. 40, No. 2, 451–455, 2004.
6. Boughrara, K., D. Zarko, R. Ibtiouen, O. Touhami, and A. Rezzoug, "Magnetic field analysis of inset and surface-mounted permanent-magnet synchronous motor using Schwarz-Christoffel transformation," *IEEE Trans. Magn.*, Vol. 45, No. 8, 3166–3168, 2009.
7. Ackermann, B. and R. Sottek, "Analytical modeling of the cogging torque in permanent magnet motors," *Elect. Eng.*, Vol. 78, No. 2, 117–125, 1994.
8. Zhu, Z. Q. and D. Howe, "Instantaneous magnetic field distribution in brushless permanent magnet dc motors, part II: Armature-reaction field," *IEEE Trans. Magn.*, Vol. 29, No. 1, 136–142, 1993.
9. Wang, X., Q. Li, S. Wang, and Q. Li, "Analytical calculation of air-gap magnetic field distribution and instantaneous characteristics of brushless dc motors," *IEEE Trans. Energy. Convers.*, Vol. 18, No. 3, 424–432, 2003.
10. Proca, A. B., A. Keyhani, A. EL-Antably, W. Lu, and M. Dai, "Analytical model for permanent magnet motors with surface

mounted magnets," *IEEE Trans. Energy Convers.*, Vol. 18, No. 3, 386–391, 2003.

11. Liu, Z. J. and J. T. Li, "Analytical solution of air-gap field in permanent magnet motors taking into account the effect of pole transition over slots," *IEEE Trans. Magn.*, Vol. 43, No. 10, 3872–3882, 2007.
12. Kumar, P. and P. Bauer, "Improved analytical model of a permanent-magnet brushless DC motor," *IEEE Trans. Magn.*, Vol. 44, No. 10, 2299–2309, 2008.
13. Afjei, E. and H. Torkaman, "The novel two-phase field assisted hybrid SRG: Magneto-static field analysis, simulation, and experimental confirmation," *Progress In Electromagnetic Research B*, Vol. 18, 25–42, 2009.
14. Babic, S. I. and C. Akiel, "Improvement of the analytical calculation of the magnetic field produced by permanent magnet rings," *Progress In Electromagnetic Research C*, Vol. 5, 71–82, 2008.
15. Ravaud, R., G. Lemarquand, V. Lemarquand, and C. Depollier, "The three exact components of the magnetic field created by a radially magnetized tile permanent magnet," *Progress In Electromagnetics Research*, Vol. 88, 307–319, 2008.
16. Bellara, A., Y. Amara, G. Barakat, and B. Dakyo, "Two-dimensional exact analytical solution of armature reaction filed in slotted surface mounted PM radial flux synchronous machines," *IEEE Trans. Magn.*, Vol. 45, No. 10, 4534–4538, 2009.
17. Lubin, T., S. Mezani, and A. Rezzoug, "Exact analytical method for magnetic field computation in the air-gap of cylindrical electrical machines considering slotting effects," *IEEE Trans. Magn.*, Vol. 46, No. 4, 1092–1099, 2010.
18. Zhu, Z. Q., L. J. Wu, and Z. P. Xia, "An accurate subdomain model for magnetic field computation in slotted surface-mounted permanent magnet machines," *IEEE Trans. Magn.*, Vol. 46, No. 4, 1100–1115, 2010.
19. Vaseghi, B., N. Takorabet, and F. Meibody-Tabar, "Transient finite element analysis of induction machine with stator winding turn fault," *Progress In Electromagnetic Research*, Vol. 95, 1–18, 2009.
20. Meeker, D. C., *Finite Element Method Magnetics*, Version 4.2, April 1, 2009 Build, http://www.femm.info.